Research Square

Preprints are preliminary reports that have not undergone peer review.
They should not be considered conclusive, used to inform clinical practice,
or referenced by the media as validated information.

Retinal Arteriolar Vessel Density and Thalamic T2 Hyperintensity in Arterial Hypertension: An Oculomics Study Using Automated Fundus Image Analysis

Constantin Geis

constantingeis@gmail.com

Palade University of Medicine, Science, and Technology of Targu Mures

Márta Germán-Salló

Palade University of Medicine, Science, and Technology of Targu Mures

Beáta Baróti

Palade University of Medicine, Science, and Technology of Targu Mures

Tünde Pál

Palade University of Medicine

Zoltán Preg

Palade University of Medicine, Science, and Technology of Targu Mures

Enikő Nemes-Nagy

Palade University of Medicine

Henrik Haba

Hatieganu University of Medicine and Pharmacy

Lajos Csincsik

Queen's University Belfast

Robert G. Tripon

Palade University of Medicine, Science, and Technology of Targu Mures

Research Article

Keywords: AutoMorph, oculomics, retinal vessel density, cerebral small vessel disease, thalamus, T2 hyperintensity

Posted Date: November 23rd, 2026

DOI: https://doi.org/10.21203/rs.3.rs-11713622/v1

License: This work is licensed under a Creative Commons Attribution 4.0 International License.
Read Full License

Additional Declarations: No competing interests reported.

Abstract

We retrospectively examined whether automatically derived retinal vascular parameters are associated with the extent of thalamic T2 hyperintensity on magnetic resonance imaging (MRI) in hypertensive patients. In 42 consecutively enrolled hypertensive patients who underwent 1.5 T MRI and colour fundus photography within seven days, the thalamic T2-hyperintense area fraction (T2HAF) was quantified on three axial T2-weighted slices with ImageJ, using a fixed threshold, by a radiologist blinded to the retinal data. Fundus photographs were analysed with AutoMorph. Associations between T2HAF and 11 retinal vascular parameters were assessed with generalised estimating equations (GEE) clustered by patient and adjusted for age and sex; multiplicity was controlled with the Benjamini–Hochberg false discovery rate (FDR). Of 84 photographs, 44 (28 patients) were gradable. Higher T2HAF was associated with lower arteriolar vessel density ($\beta = -4.5 \times 10^{-4}$ per percentage point, 95% CI − 6.7 to − 2.2 × 10^{-4}; $P < 0.001$; $q < 0.001$) and remained robust after small-sample correction and in sensitivity analyses. Inverse associations with fractal dimension ($P = 0.012$) and with the central retinal arteriolar equivalent in zones B ($P = 0.040$) and C ($P = 0.048$) did not remain significant after FDR correction. The magnification-independent arteriole-to-venule ratio was also inversely associated with T2HAF (zone C: $P = 0.001$). These hypothesis-generating findings suggest that automated fundus image analysis may offer a non-invasive approach for studying thalamic T2 hyperintensity and, potentially, thalamic small vessel pathology; they warrant validation in larger, controlled cohorts with multisequence MRI. Step-by-step AutoMorph and ImageJ protocols are provided.

Introduction

During embryonic development, both the retina and the optic nerve are derived from the diencephalon; both structures are therefore part of the central nervous system (CNS) [1]. The thalamus, as part of the diencephalon and a key relay station, is involved in arousal, mood, nociception and sensory, motor and cognitive functions, depending on the nucleus involved [2]. Consequently, the signs and symptoms of thalamic pathology vary with the affected vascular territory [2].

The retinal microvasculature is composed of non-fenestrated endothelial cells and pericytes. Its structural integrity is crucial for maintaining the inner blood–retina barrier, which functions analogously to the blood–brain barrier [1]. The retina and the brain share comparable neural and microvascular characteristics [3]. Chronic arterial hypertension damages the retinal microvasculature and thickens the arteriolar wall, leading to an increased wall-to-lumen ratio [4]; an increased retinal arteriolar wall-to-lumen ratio has also been described in patients with cerebral small vessel disease (CSVD) [5]. In the brain, the mechanisms of hypertensive CSVD include arteriolosclerosis and lipohyalinosis, in which smooth muscle cells proliferate, degenerate and are eventually replaced by fibroblasts and collagen. This results in sclerosis and a reduced lumen diameter, leading to reduced tissue perfusion [6]. The small perforating vessels supplying the thalamus, which are typically affected by lipohyalinosis, measure 40–300 µm [6], whereas retinal arterioles measure 50–100 µm [7], i.e. both vascular beds have comparable calibres.

Given the similarities in embryonic origin, structural characteristics, arteriolar size and shared pathophysiological processes, the retina may provide a window into thalamic small vessel pathology, a concept that is central to the emerging field of oculomics [8]. Several retinal vascular parameters have been associated with systemic vascular and neurological diseases. Fractal dimension expresses the overall branching complexity of the retinal vasculature and is reduced in patients with stroke and white matter lesions [9, 10]; lower arteriolar fractal dimension has also been associated with cerebral microbleeds [11]. Vessel density describes the proportion of the measured area occupied by retinal vessels; retinal capillary vessel density measured with optical coherence tomography angiography (OCTA) was lower in patients with CSVD in unadjusted analyses and decreased with increasing CSVD burden [12]. Vascular tortuosity describes the deviation of a vessel's course from a straight line [11]; increased tortuosity has been associated with hypertension, angina, myocardial infarction and stroke [13]. The central retinal arteriolar equivalent (CRAE) and central retinal venular equivalent (CRVE) summarise the average calibre of arterioles and venules, respectively, in a predefined peripapillary region [14, 15]. A larger venular and a smaller arteriolar calibre are associated with an increased risk of atherosclerotic cardiovascular events [14], and a reduced CRAE has been linked to arterial hypertension and lacunar infarction [14, 16].

To investigate these parameters in the context of thalamic pathology, we used AutoMorph, a fully automated, open-source, deep-learning-based pipeline that quantifies retinal vessel morphology from colour fundus photographs [17].

The primary aim of this exploratory study was to examine whether retinal vascular parameters measured with AutoMorph show a graded association with the extent of thalamic T2 hyperintensity, quantified on MRI as the thalamic T2-hyperintense area fraction, in patients with arterial hypertension. In hypertensive patients, such hyperintensities are frequently of presumed vascular origin, although T2 hyperintensity alone is not specific [18]. The study was designed to assess an exposure–response relationship across the range of thalamic T2 hyperintensity rather than to compare patients with healthy individuals.

A secondary aim was to facilitate the use of open-source tools in oculomics by providing step-by-step protocols for AutoMorph and for the ImageJ-based quantification of the thalamic T2-hyperintense area.

Methods

Study design and participants

This retrospective, cross-sectional, single-centre study was conducted in Targu Mures, Romania, at the George Emil Palade University of Medicine, Pharmacy, Science, and Technology of Targu Mures (UMFST) and the County Emergency Clinical Hospital of Targu Mures (ECH), and is reported in accordance with the STROBE statement [19]. Patients were examined between October 2016 and September 2017. Patients with arterial hypertension, confirmed by prior cardiological evaluation at the Cardiovascular Rehabilitation Clinic of the ECH, who underwent cerebral MRI at the Radiology and Medical Imaging

Laboratory of the ECH and colour fundus photography at the Department of Ophthalmology of the UMFST were enrolled consecutively, without selection based on MRI findings. MRI and fundus photography were performed within seven days of each other in all patients; individual intervals in days could not be retrieved retrospectively.

Inclusion criteria were (i) age ≥ 18 years, (ii) arterial hypertension, (iii) non-contrast cerebral MRI including axial T2-weighted images and (iv) colour fundus photographs of both eyes. Exclusion criteria were media opacities precluding fundus imaging, retinal vascular disease (diabetic retinopathy, retinal vein or artery occlusion), glaucoma, previous retinal laser treatment and previous vitreoretinal surgery.

Of 42 eligible patients (84 eyes, one colour fundus photograph per eye), 28 patients with at least one gradable photograph formed the analysed cohort (Fig. 1).

MRI acquisition and quantification of thalamic T2 hyperintensity

All patients underwent non-contrast cerebral MRI on a 1.5 T GE Optima MR450w system at the Radiology and Medical Imaging Laboratory of the ECH. The axial T2-weighted sequence was acquired with a repetition time/echo time of 4398/102 ms, a slice thickness of 5.0 mm, an interslice gap of 2 mm and an acquisition matrix of 288 × 224. The exposure was identified and quantified exclusively on the axial T2-weighted images. T1-weighted and FLAIR images were available but were not used for a systematic multisequence lesion classification; recent infarcts, lacunes, enlarged perivascular spaces, gliosis, demyelination and artefacts were therefore not classified separately according to the STRIVE neuroimaging standards [18]. To reflect this, the MRI measure is referred to as the thalamic T2-hyperintense area fraction (T2HAF) rather than as a radiologically confirmed microvascular lesion burden. Image selection and analysis were performed by one radiologist with 10 years of experience (B.B.), who was blinded to the retinal image analysis.

T2HAF was quantified with ImageJ (version 1.52d); the complete protocol is provided in Online Resource 1, and the procedure is illustrated in Fig. 2. Exactly three axial T2-weighted slices passing through the basal ganglia and thalami were analysed in every patient. The slices were viewed in RadiAnt with a standardised window setting (640/1280) and exported as uncompressed BMP files of identical size for all patients (512 × 515 pixels; in-plane resolution approximately 0.47 mm per pixel, corresponding to a field of view of approximately 240 mm). On each slice, the left and right thalami were delineated manually using standard anatomical boundaries (Online Resource 1). Brightness, contrast and threshold values were established once by the radiologist during an initial calibration and then kept constant for all images, without per-image adjustment; within each traced thalamus, the fixed threshold selected the T2-hyperintense pixels, which were measured with the “Limit to threshold” option. For each slice and side, the T2-hyperintense area fraction was calculated as 100 × threshold-selected pixels / thalamic pixels. The three slice-level values were averaged for each thalamus, and the left and right means were averaged to obtain the patient-level T2HAF (%). T2HAF is therefore a two-dimensional, slice-sampled area fraction measured on consistently processed raster images; it is not a volumetric measure and

does not quantify absolute signal intensity. No formal intra- or inter-rater reproducibility assessment was performed.

Fundus photography and automated retinal vascular analysis

Colour fundus photography was performed after pupil dilation with one drop of tropicamide 1% (10 mg/ml) with a Carl Zeiss Visucam 500 fundus camera (45° field; image resolution 2124 × 2056 pixels) at the Department of Ophthalmology of the UMFST. One photograph per eye was available (disc-centred, n = 83; macula-centred, n = 1). All 84 photographs were processed with AutoMorph (GitHub repository rmaphoh/AutoMorph, version of 3 July 2024, commit 11bd416; the quality-grading, segmentation and feature-extraction modules are unchanged in later versions) in Google Colab with GPU acceleration (NVIDIA Tesla T4; Python 3), using the pretrained model weights distributed with the repository without retraining; the step-by-step workflow is provided in Online Resource 2. AutoMorph comprises image pre-processing, automated image-quality grading, vessel segmentation with artery–vein classification, optic disc and cup segmentation, and feature measurement [17]. For quality grading, an ensemble of eight deep-learning models classifies each image as good, usable or reject; in accordance with the default AutoMorph settings, images graded as good, and images graded as usable with a mean predicted probability of reject below 0.25, were analysed, and all other images were excluded as ungradable. The resolution parameter was set to 1, so that all calibre and width measurements are expressed in pixels and were not converted to micrometres. The binary vessel maps, artery–vein classification maps and optic disc segmentations of all included images were visually inspected by the first author for gross segmentation errors; no segmentation was corrected and no image was excluded on this basis. Features were taken from the disc-centred AutoMorph output for the 83 disc-centred photographs and from the macula-centred output for the single macula-centred photograph.

The following parameters were analysed: fractal dimension, arteriolar and venular vessel density, arteriolar and venular average width and arteriolar and venular distance tortuosity, all measured over the whole image, and CRAE and CRVE calculated with the revised Parr–Hubbard (Knudtson) formulas [20] in zone B (0.5–1 optic disc diameters from the disc margin) and zone C (0.5–2 disc diameters), as implemented in AutoMorph and in established software such as SIVA (Fig. 3) [15, 17, 21]. Fractal dimension is dimensionless; vessel density is the proportion of the measured area occupied by vessel pixels; distance tortuosity is the ratio of vessel arc length to chord length, averaged over all vessel segments of the image (1 for a straight vessel).

Ocular magnification. Retinal dimensions measured on fundus photographs in pixels depend on ocular magnification, which varies with axial length and refraction [22]. Because these data were not available for this retrospective cohort, absolute calibres (CRAE, CRVE, average widths) could not be corrected. We therefore additionally analysed the arteriole-to-venule ratio (AVR = CRAE/CRVE) for zones B and C as a post hoc sensitivity analysis: because arterioles and venules of the same image are subject to the same magnification, the ratio is independent of ocular magnification. Fractal dimension and vessel density are dimensionless measures and are expected to be considerably less sensitive to magnification than

absolute calibres; they depend on image field and resolution, which were identical for all participants because a single camera and acquisition protocol were used.

Statistical analysis

Analyses were performed in R (version 4.5.2) with the packages geepack (version 1.3.13) [23] and lme4 (version 1.1.37) [24]. Patient-level characteristics (age, sex, T2HAF) are reported for the 28 patients, and retinal parameters for the 44 eyes. Normality was assessed with the Shapiro–Wilk test. Continuous variables are shown as mean (SD) and range, or median [interquartile range] for skewed variables, and categorical variables as n (%). For descriptive purposes, patients were divided at the patient-level median T2HAF into higher- and lower-T2HAF groups. Patient-level variables were compared with the two-sample t-test or Fisher's exact test, and eye-level retinal parameters with GEE models containing the group indicator, which account for the correlation between fellow eyes [25].

The association between T2HAF (continuous, per percentage point; independent variable) and each retinal parameter (dependent variable) was assessed with linear GEE models (Gaussian distribution, identity link, exchangeable working correlation, patient as the clustering variable) with robust sandwich standard errors [23, 25]; complete model results are given in Online Resource 3. All models were adjusted for age and sex, which were selected on the basis of prior knowledge as established determinants of retinal vessel calibre; the covariate set was restricted to these two variables because of the small number of patients. No statistical analysis plan was registered; the age- and sex-adjusted model was the model of the original analysis, and all additional analyses were sensitivity analyses. Hypertension was present in all patients by design and could therefore not be included as a covariate. Because no single primary retinal outcome had been prespecified, all 11 parameters were treated as one family of tests, and P values were adjusted with the Benjamini–Hochberg false discovery rate (FDR) procedure [26]. Both unadjusted P values and FDR-adjusted q values are reported; associations with $q < 0.05$ were considered statistically robust.

Because robust standard errors can be biased downwards when the number of patients is small, the main associations were additionally tested with the Mancl–DeRouen bias-corrected covariance estimator [27], with a nonparametric cluster bootstrap resampling patients (4000 replicates) and with linear mixed models with a random intercept for patient. Because T2HAF was right-skewed, models were also fitted with log-transformed T2HAF, and the influence of individual patients was examined by excluding the patient with the largest T2HAF (24.6%) and by leave-one-patient-out re-estimation. In an additional sensitivity analysis, the models were also adjusted for the vertical cup-to-disc ratio as a marker of optic nerve head morphology. To assess selection related to image quality, patients without any gradable photograph were compared with the analysed patients, and patients with both eyes analysed with patients with only one gradable eye (Welch t-test or two-sample t-test, Fisher's exact test and Mann–Whitney U test). Statistical significance was set at a two-sided $P < 0.05$.

Sample size. The cohort comprised all eligible patients with available data, and no a priori sample size calculation was performed. A sensitivity power analysis indicated that, with 28 patients, three predictors, $\alpha = 0.05$ and 80% power, the minimal detectable partial correlation was $|r| \approx 0.50$ (partial $R^2 \approx 0.25$). Given an intra-patient correlation of approximately 0.8, the 44 eyes correspond to an effective sample size of approximately 30 independent observations; smaller associations may therefore have been missed.

Results

Of the 84 photographs from 42 patients, 40 photographs were ungradable: both photographs of 14 patients and one photograph of 12 patients. The analysed cohort therefore comprised 44 eyes of 28 patients, of whom 16 contributed both eyes and 12 one eye (Fig. 1). Patients with both eyes analysed and patients with one gradable eye did not differ significantly in age (70.0 ± 4.0 vs 68.9 ± 5.3 years, P = 0.55), male sex (9/16 vs 3/12, P = 0.14) or T2HAF (median 4.3% vs 6.5%, P = 0.28). Likewise, the 14 patients without any gradable photograph did not differ significantly from the 28 analysed patients in age (72.4 ± 4.8 vs 69.5 ± 4.6 years, P = 0.094; age unavailable for two excluded patients), male sex (5/14 vs 12/28, P = 0.75) or T2HAF (median 4.0% vs 5.5%, P = 0.20) (Online Resource 4, Table S13).

The 28 patients (12 men, 42.9%) were aged 59–79 years (mean 69.5, SD 4.6). T2HAF was right-skewed (Shapiro–Wilk P < 0.001), with a median of 5.45% (IQR 3.07–9.19%; range 1.35–24.59%). Left and right thalamic T2HAF values were correlated (Spearman $\rho = 0.63$, P < 0.001) without a systematic side difference (Wilcoxon P = 0.27). The higher- and lower-T2HAF groups (14 patients each) did not differ in age or sex. Eyes of patients with higher T2HAF had lower arteriolar vessel density (P < 0.001) and fractal dimension (P = 0.037) than eyes of patients with lower T2HAF, whereas the differences in CRAE did not reach significance after accounting for inter-eye correlation (zone B, P = 0.057; zone C, P = 0.114) (Table 1).

Table 1
Characteristics of the analysed cohort, overall and by patient-level median T2HAF (5.45%)

Variable	Total cohort	Higher T2HAF (> median)	Lower T2HAF (≤ median)	P
Patient level				
Patients, n	28	14	14	
Eyes analysed, n	44	21	23	
Patients with both eyes analysed, n (%)	16 (57.1)	7 (50.0)	9 (64.3)	0.704
Age, years, mean (SD); range	69.5 (4.6); 59.0–79.0	69.8 (4.6); 62.0–79.0	69.3 (4.7); 59.0–75.0	0.778
Male sex, n (%)	12 (42.9)	7 (50.0)	5 (35.7)	0.704
Arterial hypertension, n (%)	28 (100)	14 (100)	14 (100)	–
T2HAF, %, median [IQR]; range	5.45 [3.07–9.19]; 1.35–24.59	9.59 [7.67–11.79]; 5.57–24.59	3.02 [2.10–3.31]; 1.35–5.33	–
Eye level				
Arteriolar vessel density	0.0320 (0.0047); 0.0218–0.0421	0.0299 (0.0054); 0.0218–0.0421	0.0340 (0.0029); 0.0292–0.0396	< 0.001
Venular vessel density	0.0363 (0.0053); 0.0273–0.0487	0.0354 (0.0058); 0.0273–0.0476	0.0371 (0.0047); 0.0296–0.0487	0.324
Arteriolar average width (px)	88.5 (5.8); 78.7–102.6	86.9 (5.6); 78.7–98.2	89.9 (5.6); 79.0–102.6	0.172
Venular average width (px)	103.9 (8.5); 80.9–121.2	103.9 (8.3); 89.2–117.7	103.9 (8.9); 80.9–121.2	0.904
Arteriolar distance tortuosity	5.49 (3.62); 1.13–15.64	5.41 (4.62); 1.13–15.64	5.56 (2.47); 1.16–9.97	0.999
Venular distance tortuosity	4.80 (2.91); 1.65–14.30	4.96 (3.03); 1.65–11.99	4.66 (2.86); 2.04–14.30	0.899
CRAE zone B (px)	231.9 (25.2); 177.9–298.2	223.5 (23.4); 177.9–282.3	239.7 (24.8); 198.8–298.2	0.057
CRVE zone B (px)	300.0 (34.1); 219.0–374.3	300.9 (35.2); 251.1–374.3	299.1 (33.9); 219.0–344.4	0.722

Patient-level variables refer to 28 patients and eye-level variables to 44 eyes. Continuous variables are mean (SD); range, or median [interquartile range]; range. P values: two-sample t-test (age), Fisher's exact test (categorical variables) and GEE with exchangeable correlation clustered by patient (eye-level parameters). T2HAF, thalamic T2-hyperintense area fraction (% of thalamic area); CRAE/CRVE, central retinal arteriolar/venular equivalent; px, pixels

Variable	Total cohort	Higher T2HAF (> median)	Lower T2HAF (≤ median)	P
Patient level				
CRAE zone C (px)	247.3 (26.3); 187.0–302.4	240.1 (28.0); 187.0–302.4	253.8 (23.4); 213.6–296.9	0.114
CRVE zone C (px)	328.2 (37.3); 232.8–406.5	330.8 (39.6); 266.0–406.5	325.8 (35.7); 232.8–378.9	0.707
Fractal dimension	1.481 (0.026); 1.435–1.531	1.473 (0.028); 1.435–1.524	1.489 (0.020); 1.458–1.531	0.037

Patient-level variables refer to 28 patients and eye-level variables to 44 eyes. Continuous variables are mean (SD); range, or median [interquartile range]; range. P values: two-sample t-test (age), Fisher's exact test (categorical variables) and GEE with exchangeable correlation clustered by patient (eye-level parameters). T2HAF, thalamic T2-hyperintense area fraction (% of thalamic area); CRAE/CRVE, central retinal arteriolar/venular equivalent; px, pixels

Associations between T2HAF and retinal vascular parameters

Results for all 11 parameters are shown in Table 2; Fig. 4 shows the four parameters with $P < 0.05$, and scatterplots of all parameters are provided in Online Resource 4. Higher T2HAF was associated with lower arteriolar vessel density ($\beta = -4.5 \times 10^{-4}$ per percentage point, 95% CI − 6.7 to − 2.2×10^{-4}; $P < 0.001$; $q < 0.001$). This corresponds to a decrease of 2.2×10^{-3} per 5 percentage points of T2HAF, i.e. approximately 7% of the cohort mean arteriolar vessel density (0.032). Higher T2HAF was also associated with lower fractal dimension ($\beta = -1.6 \times 10^{-3}$, 95% CI − 2.9 to − 0.4×10^{-3}; $P = 0.012$; $q = 0.066$), lower CRAE in zone B ($\beta = -1.27$ pixels, 95% CI − 2.47 to − 0.06; $P = 0.040$; $q = 0.133$) and lower CRAE in zone C ($\beta = -1.24$ pixels, 95% CI − 2.46 to − 0.01; $P = 0.048$; $q = 0.133$); these three associations did not remain significant after FDR correction. No other parameter was associated with T2HAF (all $P \geq 0.08$; Table 2).

With respect to the covariates, male sex was associated with larger CRAE in zone B ($\beta = 16.5$ pixels, 95% CI 0.5–32.5; $P = 0.043$) and zone C ($\beta = 18.2$ pixels, 95% CI 0.2–36.2; $P = 0.047$), larger CRVE in zone C ($\beta = 24.6$ pixels, 95% CI 2.6–46.6; $P = 0.029$) and larger venular average width ($\beta = 6.7$ pixels, 95% CI 1.8–11.6; $P = 0.007$). Age was not associated with any parameter. The complete models, including intercepts and covariates, are presented in Online Resource 3.

Table 2
Associations between T2HAF and retinal vascular parameters (GEE, adjusted for age and sex; 44 eyes of 28 patients)

Retinal parameter	Mean (SD)	β per percentage point of T2HAF (95% CI)	P	q (FDR)
Arteriolar vessel density	**0.0320 (0.0047)**	**−4.5 (− 6.7 to − 2.2) × 10^{-4}**	**< 0.001**	**< 0.001**
Venular vessel density	0.0363 (0.0053)	−1.0 (− 3.8 to 1.8) × 10^{-4}	0.471	0.576
Arteriolar average width (px)	88.5 (5.8)	−0.20 (− 0.56 to 0.16)	0.278	0.437
Venular average width (px)	103.9 (8.5)	0.02 (− 0.46 to 0.49)	0.938	0.938
Arteriolar distance tortuosity	5.49 (3.62)	−0.06 (− 0.24 to 0.12)	0.528	0.581
Venular distance tortuosity	4.80 (2.91)	−0.11 (− 0.26 to 0.03)	0.118	0.216
CRAE zone B (px)	231.9 (25.2)	−1.27 (− 2.47 to − 0.06)	0.040	0.133
CRVE zone B (px)	300.0 (34.1)	0.92 (− 1.20 to 3.05)	0.394	0.542
CRAE zone C (px)	247.3 (26.3)	−1.24 (− 2.46 to − 0.01)	0.048	0.133
CRVE zone C (px)	328.2 (37.3)	1.55 (− 0.19 to 3.29)	0.080	0.176
Fractal dimension	1.481 (0.026)	−1.6 (− 2.9 to − 0.4) × 10^{-3}	0.012	0.066

β, change in the parameter per percentage-point increase in T2HAF, with robust (sandwich) 95% CI; q (FDR), Benjamini–Hochberg false discovery rate across the 11 parameters; bold, association that remained significant after FDR correction (q < 0.05). Full models including intercept, age and sex are given in Online Resource 3; robustness analyses in Online Resource 4

Robustness of the associations

The association between T2HAF and arteriolar vessel density remained significant after small-sample correction (P = 0.007), in the cluster bootstrap (P = 0.004), in the linear mixed model (P = 0.010), with log-transformed T2HAF (P < 0.001), after exclusion of the patient with the largest T2HAF (β = −5.4 × 10^{-4}, P < 0.001), in every leave-one-patient-out analysis (all P < 0.001) and after additional adjustment for the vertical cup-to-disc ratio (P < 0.001). For fractal dimension, the small-sample-corrected P value was 0.049; the association remained significant with log-transformed T2HAF (P = 0.010), after exclusion of the patient with the largest T2HAF (P = 0.024) and in all leave-one-out analyses, but not in the cluster bootstrap (P = 0.061) or the linear mixed model (P = 0.093). The CRAE associations were less stable: the small-sample-corrected P values were 0.092 (zone B) and 0.100 (zone C), the associations were not significant in the cluster bootstrap, the linear mixed model or with log-transformed T2HAF (all P ≥ 0.07),

and significance was lost after exclusion of the patient with the largest T2HAF (both P = 0.22) and in 11 (zone B) and 17 (zone C) of the 28 leave-one-out analyses. Adjustment for the vertical cup-to-disc ratio did not materially change any estimate (Online Resource 4).

In the magnification-independent analysis, higher T2HAF was associated with a lower AVR in zone B (β = -6.1×10^{-3}, 95% CI − 10.8 to -1.5×10^{-3}; P = 0.010) and zone C (β = -7.0×10^{-3}, 95% CI − 11.3 to -2.8×10^{-3}; P = 0.001); both associations remained significant after small-sample correction (P = 0.041 and P = 0.011, respectively). After exclusion of the patient with the largest T2HAF, the corresponding P values were 0.044 (zone B) and 0.053 (zone C), and the zone C association remained significant in 27 of the 28 leave-one-out analyses.

Robustness analyses and scatterplots for all parameters are presented in Online Resource 4.

Discussion

In hypertensive patients, a greater thalamic T2-hyperintense area fraction on MRI was associated with lower retinal arteriolar vessel density measured automatically on colour fundus photographs. This association remained significant after correction for multiple testing and small-sample correction and was not driven by individual patients. Associations with lower fractal dimension and lower CRAE were in the same direction but did not survive correction for multiple testing, whereas the magnification-independent AVR was inversely associated with T2HAF. Taken together, the findings suggest that the retinal arteriolar network, rather than the venular network, is the more likely retinal correlate of thalamic T2 hyperintensity. Because thalamic hyperintensities were not classified by lesion type, and because the cohort was small and lacked a control group, these findings require confirmation in larger studies with multisequence MRI.

Studies of retinal vascular parameters in CSVD have so far yielded heterogeneous results, and most were small and used non-standardised methods [28]. For example, in a Singaporean cohort, narrower arterioles, wider venules and lower arteriolar fractal dimension were associated with cerebral microbleeds but not with lacunar infarcts or white matter lesion volume [11], and in the population-based Rotterdam Scan Study, wider venules, but not narrower arterioles, were associated with progression of white matter lesions and incident lacunar infarcts [29]. Retinal changes in relation to thalamic pathology have rarely been studied, and the available data come from OCTA in thalamic infarction [3]. To our knowledge, this is the first study to examine retinal vascular parameters derived automatically from conventional colour fundus photographs in relation to a quantitative MRI measure of thalamic T2 hyperintensity.

Vessel density reflects the proportion of retinal area occupied by vessels and therefore integrates both vessel calibre and the number of visible vessel segments. A lower arteriolar vessel density is consistent with microvascular rarefaction, i.e. a reduced number of perfused arterioles and capillaries, which is a recognised feature of the hypertensive microcirculation [30]. Similar processes are thought to underlie hypertensive CSVD, in which arteriolosclerosis and lipohyalinosis of perforating arteries lead to luminal

narrowing, chronic hypoperfusion and ischaemic lesions in deep grey matter structures such as the thalamus [6]. In line with our findings, retinal capillary vessel density measured with OCTA has been reported to decrease with increasing CSVD burden [12], and reduced density of the superficial and intermediate capillary plexuses together with thinning of the retinal nerve fibre and ganglion cell–inner plexiform layers has been described in patients with thalamic infarction, where these changes correlated with infarct volume [3]. Our data extend these observations to the larger arterioles visible on conventional fundus photographs and to a continuous MRI measure of thalamic T2 hyperintensity. In hypertensive patients, such hyperintensity is likely to be largely of vascular origin, but this was not confirmed by lesion classification in the present study.

Retinal arteriolar narrowing is a classic sign of hypertensive retinopathy and reflects vascular remodelling with intimal thickening, medial hyperplasia and sclerosis [31]. Reduced CRAE and increased CRVE have been associated with lacunar infarction, stroke and cardiovascular events [14, 16, 32], and parallel hypertensive changes of the cerebral perforating arteries [6] and of the retinal arterioles [31] provide a plausible link to thalamic small vessel pathology. In our cohort, the CRAE associations were directionally consistent with this concept but were imprecise and did not survive correction for multiple testing. One likely contributor is measurement error: CRAE is expressed in pixels and could not be corrected for ocular magnification, which varies with axial length and refraction [22]. Such error is unlikely to be related to T2HAF; it reduces precision but is not expected to create spurious associations. Consistent with this interpretation, the AVR, which is independent of magnification because arterioles and venules of the same image are equally affected, showed an inverse association with T2HAF that was more robust than that of CRAE, although the zone C association was borderline after exclusion of the most extreme patient ($P = 0.053$). Because the AVR combines arteriolar and venular calibre, a lower AVR can result from arteriolar narrowing, venular widening, or both; in our data, CRAE showed a non-significant decrease and CRVE a non-significant increase with T2HAF. The AVR finding should therefore be interpreted as supportive rather than confirmatory.

Fractal dimension, a global measure of the branching complexity of the retinal vasculature, is reduced in stroke and neurodegenerative disease [9], and lower arteriolar fractal dimension has been associated with deep white matter hyperintensities in patients with minor stroke [10]; reduced fractal dimension has also been related to hypoxia [16]. The inverse association in our study is consistent with these reports, although it did not survive FDR correction and should be confirmed in larger samples. We found no association between T2HAF and tortuosity, venular density or venular calibre. Patients with ischaemic stroke have been reported to have wider venules and increased arteriolar and venular tortuosity [32]; our study had limited power to detect associations of small to moderate size. The association between male sex and larger vessel calibres, expressed in pixels, may reflect sex differences in ocular dimensions and hence magnification, rather than true differences in vessel diameter, and should not be over-interpreted.

From a clinical perspective, fundus photography is widely available, inexpensive and non-invasive, and automated open-source pipelines such as AutoMorph allow standardised quantification without specialised software licences [17], which facilitates oculomics research [8]. Our results identify arteriolar

vessel density as a promising retinal correlate of thalamic T2 hyperintensity and, potentially, of thalamic small vessel disease. Before clinical application, this requires demonstration of discriminative performance against control participants, validation in independent cohorts and longitudinal evidence that retinal changes precede or predict cerebral lesions. A practical observation is that almost half of the photographs (40/84) failed AutoMorph quality grading. Despite pharmacological mydriasis, elderly patients often have small pupils and lens opacities that do not preclude imaging but degrade image quality; future studies should use standardised acquisition protocols and, if possible, repeated imaging, to minimise data loss and the associated risk of selection bias. The protocols provided in Online Resources 1 and 2 are intended to facilitate such replication.

This study has several limitations. First, it is a retrospective, cross-sectional, single-centre study without a control group. All participants had hypertension, so our results describe a gradient across the extent of thalamic T2 hyperintensity within this population and cannot show whether retinal parameters differ from those of normotensive or lesion-free individuals; causal and temporal inferences are not possible. Because MRI and fundus photography were performed within seven days of each other, major changes in vascular status between the examinations are, however, unlikely. Second, the sample size was determined by the available cohort and no single primary outcome had been prespecified; although we controlled the FDR and applied a small-sample correction, the study was powered to detect only large associations (partial $|r| \geq 0.50$), smaller effects may have been missed, and the nominal fractal dimension and CRAE associations, which did not survive correction for multiple testing, may represent false-positive findings. Third, adjustment was limited to age and sex. Blood pressure level and duration of hypertension, antihypertensive medication, diabetes mellitus, smoking, dyslipidaemia, renal function and prior stroke were not available for the cohort, and residual confounding cannot be excluded. In particular, because blood pressure could not be taken into account, the retinal findings may reflect the overall severity of hypertensive microvascular disease rather than thalamic involvement specifically. Fourth, axial length and refraction were not available, so absolute calibres could not be corrected for ocular magnification and are reported in pixels; we addressed this partly with the AVR and with dimensionless parameters. Fifth, the MRI measure has several limitations. T2HAF was derived exclusively from axial T2-weighted images at 1.5 T; T1-weighted and FLAIR images were available but were not used for systematic lesion classification, so recent infarcts, lacunes, enlarged perivascular spaces, gliosis, demyelination and artefacts were not excluded, and T2HAF should not be equated with an aetiologically confirmed microvascular lesion burden [18]. Moreover, T2HAF is a two-dimensional area fraction from three slices of exported raster images rather than a volumetric measure, and thalamic tracing and the initial threshold calibration involved operator judgement; although all settings were subsequently kept constant and the radiologist was blinded to the retinal data, no formal reproducibility assessment was performed, and partial-volume effects at thalamic borders adjacent to cerebrospinal fluid may have contributed to the threshold-selected area (Fig. 2c). Such measurement error is unlikely to be related to the retinal parameters and would therefore be expected to attenuate rather than create associations. In addition, whole-brain markers of CSVD, such as white matter hyperintensities, lacunes outside the thalamus and microbleeds, were not rated [18], so it remains unclear whether the

associations are specific to the thalamus or reflect the overall burden of cerebral small vessel disease. Finally, 48% of photographs were excluded by automated quality grading. Excluded and analysed patients did not differ significantly in age, sex or T2HAF, although excluded patients were on average 2.9 years older (P = 0.094); selection bias therefore cannot be fully excluded. Moreover, AutoMorph has not been specifically validated in this population or with this camera, and its outputs were not compared with manual grading in this cohort.

Future studies should include age- and sex-matched control groups with and without hypertension, prespecify a primary retinal outcome (arteriolar vessel density being a candidate on the basis of the present data), record axial length and cardiovascular risk factors, classify thalamic lesions on multisequence MRI according to STRIVE criteria, quantify lesion volume on high-resolution three-dimensional MRI with assessment of reproducibility, and follow patients longitudinally.

Conclusion

In hypertensive patients, a greater thalamic T2-hyperintense area fraction on MRI was associated with lower retinal arteriolar vessel density measured automatically on colour fundus photographs, and this association was robust to correction for multiple testing. Associations with fractal dimension and arteriolar calibre were weaker. These hypothesis-generating findings suggest that automated retinal vascular analysis may offer a non-invasive approach for studying thalamic T2 hyperintensity and, potentially, thalamic small vessel pathology; they require validation in larger, controlled and longitudinal studies with multisequence MRI lesion classification.

Declarations

Competing interests:

The authors have no relevant financial or non-financial interests to disclose.

Ethical approval:

Ethical approval no. 19779 was granted by the Ethics Committee of the County Emergency Clinical Hospital of Targu Mures. All participants were informed about the study’s purpose and procedures, and consent was obtained prior to inclusion. The research was carried out in compliance with the principles outlined in the Declaration of Helsinki regarding medical studies involving human subjects.

Consent to participate:

All participants were informed about the purpose and procedures of the study, informed consent was obtained and participation was voluntary.

Consent for publication:

Not applicable.

Funding:

This study received funding from the Hungarian Academy of Sciences and the Studium Prospero Foundation through a shared grant (grant no. 346).

Author Contribution

Conceptualization: Robert G. Tripon, Lajos Csincsik, Márta Germán-Salló; Methodology: Constantin Geis, Lajos Csincsik and Robert G. Tripon; Data collection: Robert G. Tripon, Márta Germán-Salló, Beáta Baróti, Tünde Pál, Zoltán Preg, Enikő Nemes-Nagy and Henrik Haba; MRI analysis: Beáta Baróti; Retinal image analysis: Constantin Geis; Formal analysis: Constantin Geis; Writing – original draft preparation: Constantin Geis; Writing – review and editing: Constantin Geis, Lajos Csincsik, Robert G. Tripon, Márta Germán-Salló, Beáta Baróti, Tünde Pál, Zoltán Preg, Enikő Nemes-Nagy and Henrik Haba. All authors read and approved the final manuscript.

Acknowledgements:

The authors express their gratitude to the Head of Department, Associate Professor Karin U. Horvath, for facilitating patient evaluations at the Ophthalmology Clinic of Targu Mures, and to Dr. Norbert Lita for his valuable assistance in preparing the supplementary material.

Data availability:

The datasets generated or analysed during the current study are not publicly available due to patient privacy and institutional data protection regulations but are available from the corresponding author on reasonable request and subject to approval by the responsible institutional authorities.

Code availability:

The R analysis code is provided as Online Resource 5.

References

1. 1. DeBuc DC, Somfai GM, Koller A (2017) Retinal microvascular network alterations: Potential biomarkers of cerebrovascular and neural diseases. Am J Physiol Heart Circ Physiol 312:H201–H212. https://doi.org/10.1152/ajpheart.00201.2016
2. 2. Schmahmann JD (2003) Vascular syndromes of the thalamus. Stroke 34:2264–2278. https://doi.org/10.1161/01.STR.0000087786.38997.9E
3. 3. Ye C, Kwapong WR, Tao W, et al (2022) Characterization of Macular Structural and Microvascular Changes in Thalamic Infarction Patients: A Swept-Source Optical Coherence Tomography-Angiography Study. Brain Sci 12:518. https://doi.org/10.3390/brainsci12050518
4. 4. Gallo A, Mattina A, Rosenbaum D, et al (2016) Retinal arteriolar remodeling evaluated with adaptive optics camera: Relationship with blood pressure levels. Ann Cardiol Angeiol (Paris) 65:203–207. https://doi.org/10.1016/j.ancard.2016.04.021
5. 5. Abdelhak A, Huss A, Brück A, et al (2020) Optical coherence tomography-based assessment of retinal vascular pathology in cerebral small vessel disease. Neurol Res Pract 2:13. https://doi.org/10.1186/s42466-020-00062-4
6. 6. Lammie GA (2002) Hypertensive cerebral small vessel disease and stroke. Brain Pathol 12:358–370. https://doi.org/10.1111/j.1750-3639.2002.tb00450.x
7. 7. Cogan DG, Kuwabara T, Friedman E (1968) Retinal vasculature. Microvasc Res 1:115–132. https://doi.org/10.1016/0026-2862(68)90012-5
8. 8. Wagner SK, Fu DJ, Faes L, et al (2020) Insights into systemic disease through retinal imaging-based oculomics. Transl Vis Sci Technol 9:6. https://doi.org/10.1167/tvst.9.2.6
9. 9. Lemmens S, Devulder A, Van Keer K, et al (2020) Systematic Review on Fractal Dimension of the Retinal Vasculature in Neurodegeneration and Stroke: Assessment of a Potential Biomarker. Front Neurosci 14:16. https://doi.org/10.3389/fnins.2020.00016
10. 10. McGrory S, Ballerini L, Doubal FN, et al (2019) Retinal microvasculature and cerebral small vessel disease in the Lothian Birth Cohort 1936 and Mild Stroke Study. Sci Rep 9:6320. https://doi.org/10.1038/s41598-019-42534-x
11. 11. Hilal S, Ong YT, Cheung CY, et al (2014) Microvascular network alterations in retina of subjects with cerebral small vessel disease. Neurosci Lett 577:95–100. https://doi.org/10.1016/j.neulet.2014.06.024
12. 12. Wang D, Wang L, Wang J, et al (2024) Retinal structure and vessel density changes in cerebral small vessel disease. Front Neurosci 18:1288380. https://doi.org/10.3389/fnins.2024.1288380
13. 13. Tomasoni M, Beyeler MJ, Vela SO, et al (2023) Genome-wide Association Studies of Retinal Vessel Tortuosity Identify Numerous Novel Loci Revealing Genes and Pathways Associated With Ocular and Cardiometabolic Diseases. Ophthalmol Sci 3:100288. https://doi.org/10.1016/j.xops.2023.100288
14. 14. Hanssen H, Streese L, Vilser W (2022) Retinal vessel diameters and function in cardiovascular risk and disease. Prog Retin Eye Res 91:101095. https://doi.org/10.1016/j.preteyeres.2022.101095

15. 15. Gao Y, Xu L, He N, et al (2023) A narrative review of retinal vascular parameters and the applications (Part I): Measuring methods. Brain Circ 9:121–128. https://doi.org/10.4103/bc.bc_8_23
16. 16. Rim TH, Teo AWJ, Yang HHS, et al (2020) Retinal Vascular Signs and Cerebrovascular Diseases. J Neuroophthalmol 40:44–59. https://doi.org/10.1097/WNO.0000000000000888
17. 17. Zhou Y, Wagner SK, Chia MA, et al (2022) AutoMorph: Automated Retinal Vascular Morphology Quantification Via a Deep Learning Pipeline. Transl Vis Sci Technol 11:12. https://doi.org/10.1167/tvst.11.7.12
18. 18. Wardlaw JM, Smith EE, Biessels GJ, et al (2013) Neuroimaging standards for research into small vessel disease and its contribution to ageing and neurodegeneration. Lancet Neurol 12:822–838. https://doi.org/10.1016/S1474-4422(13)70124-8
19. 19. von Elm E, Altman DG, Egger M, et al (2007) The Strengthening the Reporting of Observational Studies in Epidemiology (STROBE) statement: guidelines for reporting observational studies. Lancet 370:1453–1457. https://doi.org/10.1016/S0140-6736(07)61602-X
20. 20. Knudtson MD, Lee KE, Hubbard LD, et al (2003) Revised formulas for summarizing retinal vessel diameters. Curr Eye Res 27:143–149. https://doi.org/10.1076/ceyr.27.3.143.16049
21. 21. Cheung CYL, Hsu W, Lee ML, et al (2010) A new method to measure peripheral retinal vascular caliber over an extended area. Microcirculation 17:495–503. https://doi.org/10.1111/J.1549-8719.2010.00048.X
22. 22. Bennett AG, Rudnicka AR, Edgar DF (1994) Improvements on Littmann's method of determining the size of retinal features by fundus photography. Graefes Arch Clin Exp Ophthalmol 232:361–367. https://doi.org/10.1007/BF00175988
23. 23. Halekoh U, Højsgaard S, Yan J (2006) The R package geepack for generalized estimating equations. J Stat Softw 15:1–11. https://doi.org/10.18637/jss.v015.i02
24. 24. Bates D, Mächler M, Bolker B, Walker S (2015) Fitting linear mixed-effects models using lme4. J Stat Softw 67:1–48. https://doi.org/10.18637/jss.v067.i01
25. 25. Ying GS, Maguire MG, Glynn R, Rosner B (2017) Tutorial on biostatistics: linear regression analysis of continuous correlated eye data. Ophthalmic Epidemiol 24:130–140. https://doi.org/10.1080/09286586.2016.1259636
26. 26. Benjamini Y, Hochberg Y (1995) Controlling the false discovery rate: a practical and powerful approach to multiple testing. J R Stat Soc Series B Stat Methodol 57:289–300. https://doi.org/10.1111/j.2517-6161.1995.tb02031.x
27. 27. Mancl LA, DeRouen TA (2001) A covariance estimator for GEE with improved small-sample properties. Biometrics 57:126–134. https://doi.org/10.1111/j.0006-341X.2001.00126.x
28. 28. Biffi E, Turple Z, Chung J, Biffi A (2022) Retinal biomarkers of cerebral small vessel disease: a systematic review. PLoS One 17:e0266974. https://doi.org/10.1371/journal.pone.0266974
29. 29. Ikram MK, De Jong FJ, Van Dijk EJ, et al (2006) Retinal vessel diameters and cerebral small vessel disease: the Rotterdam Scan Study. Brain 129:182–188. https://doi.org/10.1093/brain/awh688

30. 30. Feihl F, Liaudet L, Waeber B, Levy BI (2006) Hypertension: a disease of the microcirculation? Hypertension 48:1012–1017. https://doi.org/10.1161/01.HYP.0000249510.20326.72
31. 31. Wong TY, Mitchell P (2004) Hypertensive Retinopathy. N Engl J Med 351:2310–2317. https://doi.org/10.1056/NEJMra032865
32. 32. Ong YT, De Silva DA, Cheung CY, et al (2013) Microvascular structure and network in the retina of patients with ischemic stroke. Stroke 44:2121–2127. https://doi.org/10.1161/STROKEAHA.113.001741

Figures

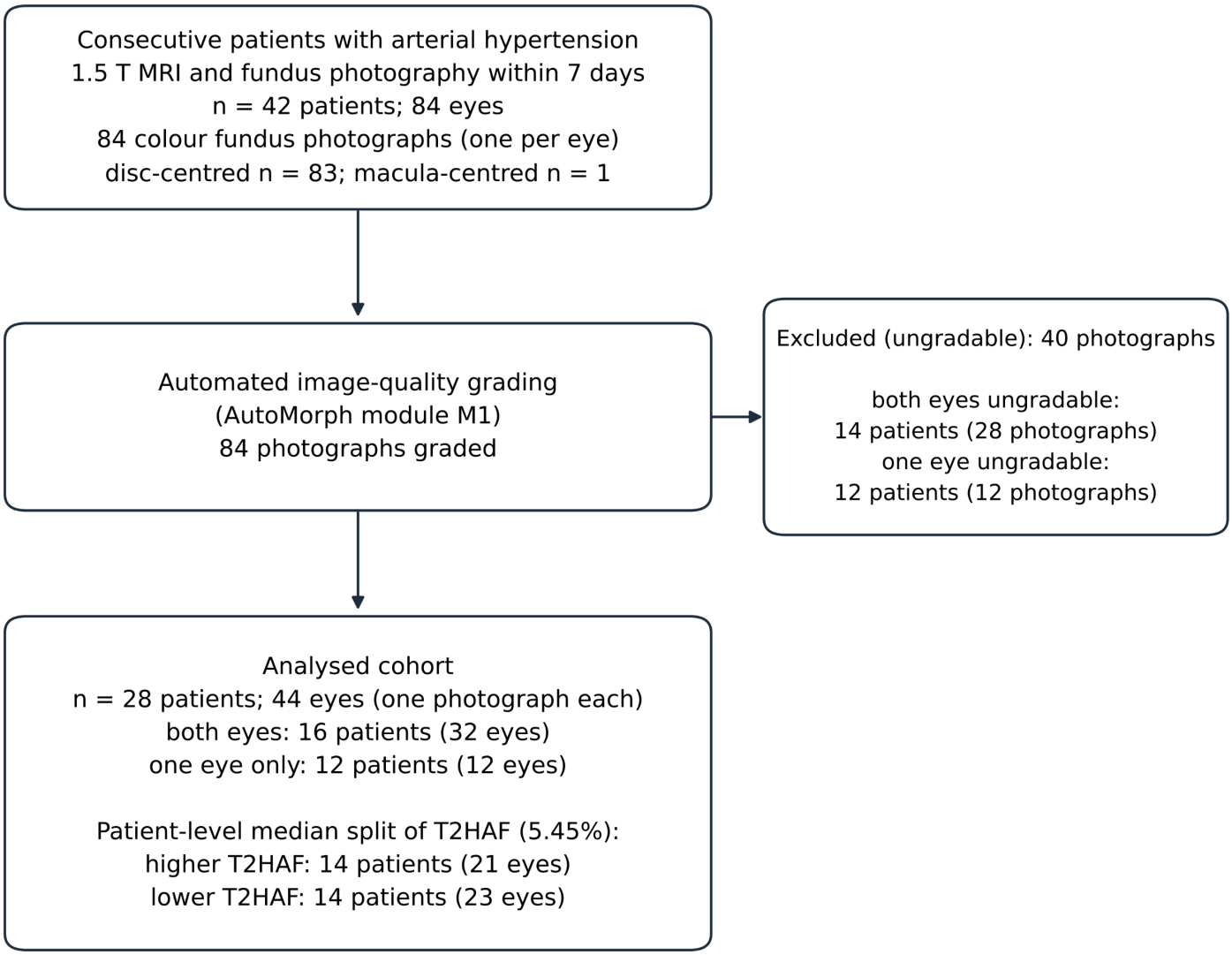


Figure 1

Flow of patients and colour fundus photographs. T2HAF, thalamic T2-hyperintense area fraction

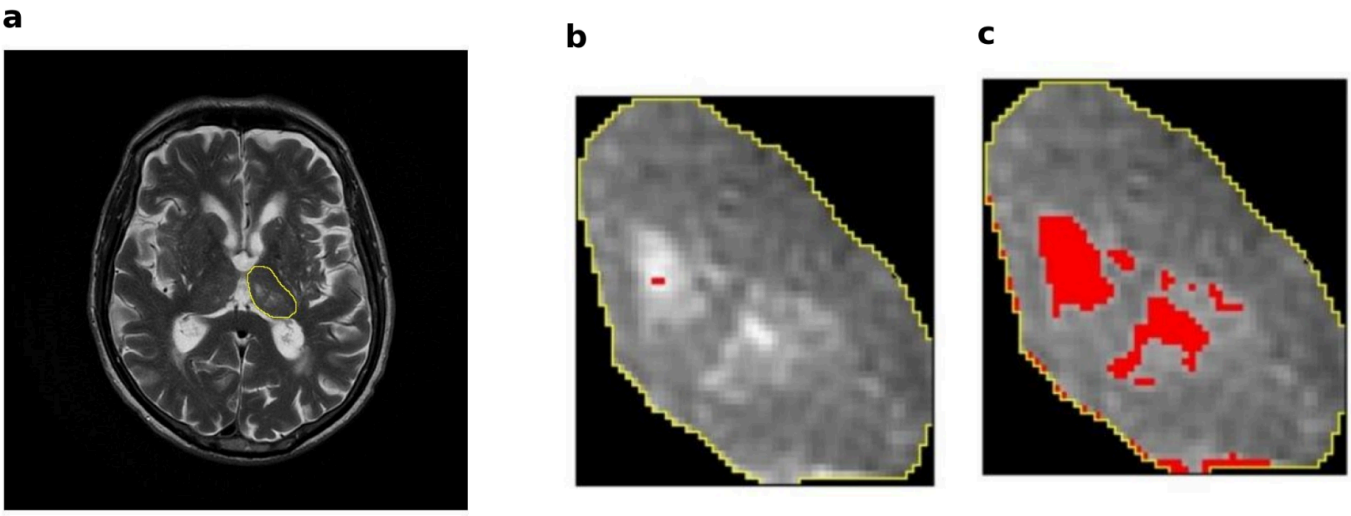


Figure 2

Quantification of the thalamic T2-hyperintense area fraction (T2HAF) in ImageJ, illustrated in a patient of the present cohort. (a) Axial T2-weighted slice at the level of the thalami with the manual outline of the left thalamus (yellow). (b, c) Isolated thalamic region of interest before (b) and after (c) application of the fixed intensity threshold; threshold-selected T2-hyperintense pixels are shown in red. T2HAF was calculated as the percentage of threshold-selected pixels within the outlined thalamus, averaged over three slices and both thalami

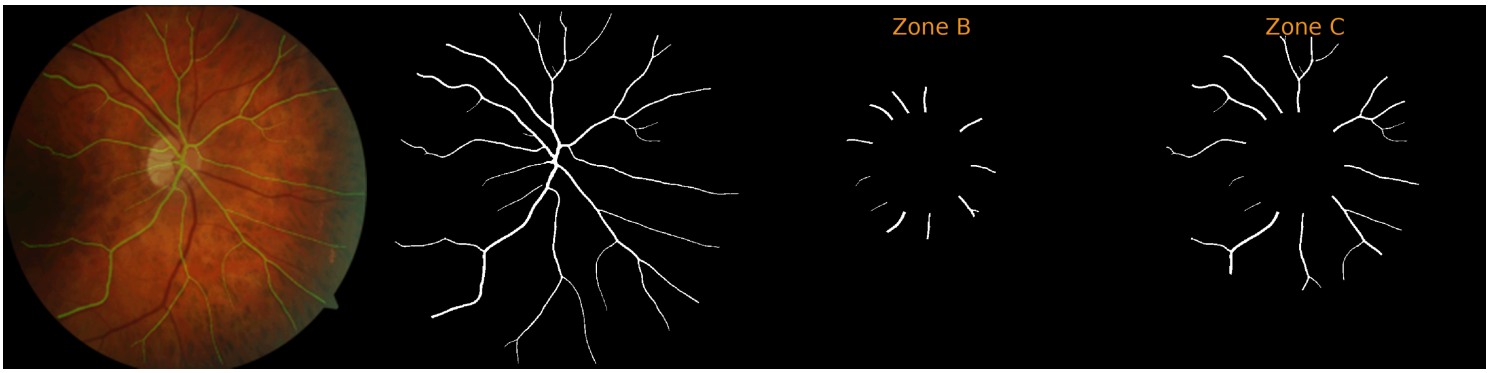


Figure 3

AutoMorph arteriolar segmentation of a right eye. From left to right: original fundus photograph with green overlay on arterioles, binary arteriolar map, binary arterioles in zone B and binary arterioles in zone C

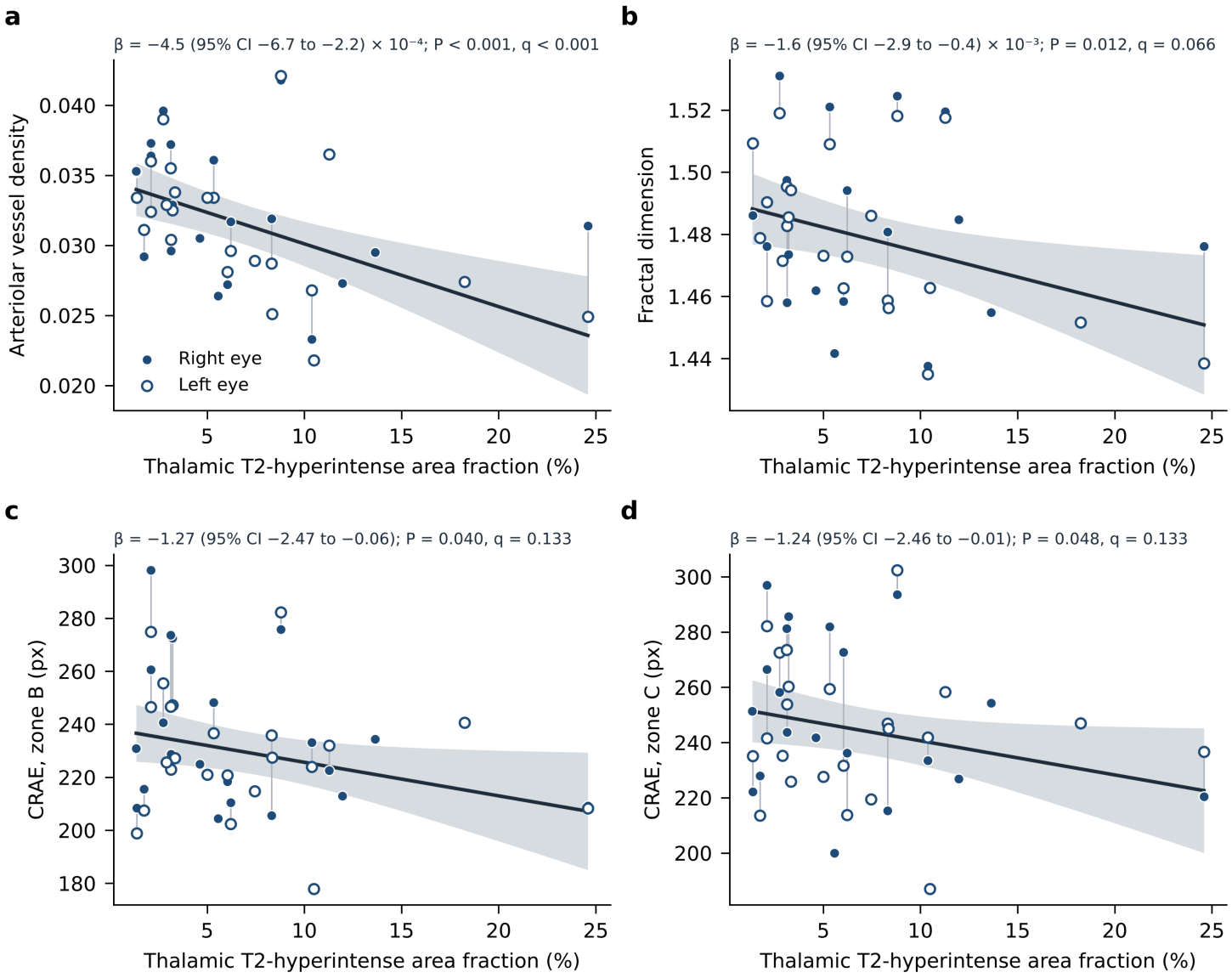


Figure 4

Associations between the thalamic T2-hyperintense area fraction (T2HAF) and (a) arteriolar vessel density, (b) fractal dimension, (c) CRAE in zone B and (d) CRAE in zone C. Points represent eyes (filled, right eye; open, left eye); fellow eyes of the same patient are connected by grey lines. The solid line and shaded band show the GEE-estimated association and its 95% confidence interval (robust standard errors), evaluated at the mean age and sex distribution of the cohort. β, change per percentage point of T2HAF; q, Benjamini–Hochberg FDR-adjusted P value across the 11 parameters

Supplementary Files

This is a list of supplementary files associated with this preprint. Click to download.

- ESM5.docx

- ESM3.docx
- ESM1.docx
- ESM4.docx
- ESM2.docx